

E-CRF: EMBEDDED CONDITIONAL RANDOM FIELD FOR BOUNDARY-CAUSED CLASS WEIGHTS CONFUSION IN SEMANTIC SEGMENTATION

Jie Zhu^{1,2} Huabin Huang³ Banghuai Li³ Leye Wang^{1,2*}

Key Lab of High Confidence Software Technologies (Peking University), Ministry of Education, China¹

School of Computer Science, Peking University, Beijing, China²

MEGVII Technology³

zhujie@stu.pku.edu.cn, {huanghuabin1994, libanghuai}@gmail.com, leyewang@pku.edu.cn

ABSTRACT

Modern semantic segmentation methods devote much effort to adjusting image feature representations to improve the segmentation performance in various ways, such as architecture design, attention mechanism, etc. However, almost all those methods neglect the particularity of class weights (in the classification layer) in segmentation models. In this paper, we notice that the class weights of categories that tend to share many adjacent boundary pixels lack discrimination, thereby limiting the performance. We call this issue *Boundary-caused Class Weights Confusion (BCWC)*. We try to focus on this problem and propose a novel method named *Embedded Conditional Random Field (E-CRF)* to alleviate it. E-CRF innovatively fuses the CRF into the CNN network as an organic whole for more effective end-to-end optimization. The reasons are two folds. It utilizes CRF to guide the message passing between pixels in high-level features to purify the feature representation of boundary pixels, with the help of inner pixels belonging to the same object. More importantly, it enables optimizing class weights from both **scale** and **direction** during backpropagation. We make detailed theoretical analysis to prove it. Besides, superpixel is integrated into E-CRF and served as an auxiliary to exploit the local object prior for more reliable message passing. Finally, our proposed method yields impressive results on ADE20K, Cityscapes, and Pascal Context datasets.

1 INTRODUCTION

Semantic segmentation plays an important role in practical applications such as autonomous driving, image editing, *etc.* Nowadays, numerous CNN-based methods (Chen et al., 2014; Fu et al., 2019; Ding et al., 2019) have been proposed. They attempt to adjust the image feature representation of the model itself to recognize each pixel correctly. However, almost all those methods neglect the particularity of class weights (in the classification layer) that play an important role in distinguishing pixel categories in segmentation models. Hence, it is critical to keep class weights discriminative. Unfortunately, CNN models have the natural defect for this. Generally speaking, most discriminative higher layers in the CNN network always have the larger receptive field, thus pixels around the boundary may obtain confusing features from both sides. As a result, these ambiguous boundary pixels will mislead the optimization direction of the model and make the class weights of such categories that tend to share adjacent pixels indistinguishable. For the convenience of illustration, we call this issue as *Boundary-caused Class Weights Confusion (BCWC)*. We take DeeplabV3+ (Chen et al., 2018a) as an example to train on ADE20K (Zhou et al., 2017) dataset. Then, we count the number of adjacent pixels for each class pair and find a corresponding category that has the most adjacent pixels for each class. Fig 1(a) shows the similarity of the class weight between these pairs in descending order according to the number of adjacent pixels. It is clear that if two categories share more adjacent pixels, their class weights tend to be more similar, which actually indicates that BCWC makes class representations lack discrimination and damages the overall segmentation performance.

*Corresponding author.

Previous works mainly aim to improve boundary pixel segmentation, but they seldom explicitly take class weights confusion *i.e.*, BCWC, into consideration ¹.

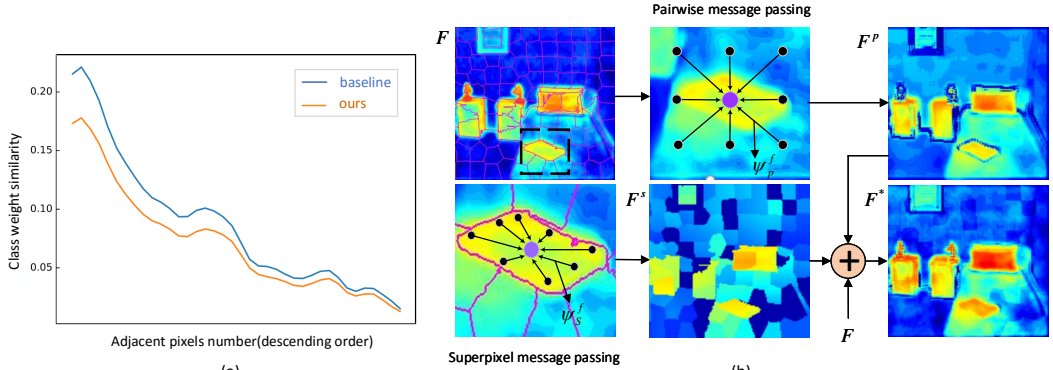


Figure 1: (a) Observations on ADE20K. We find a corresponding category that shares the most adjacent pixels for each class and calculate the similarity of their class weights. X-axis stands for the number of adjacent pixels for each class pair in descending order, and Y-axis represents the similarity of their class weights. Blue line denotes baseline model while orange line denotes E-CRF. Apparently, two categories that share more adjacent pixels are inclined to have more similar class weights, while E-CRF effectively decreases the similarity between *adjacent categories* and makes their class weights more discriminative. (b) Message passing procedure of E-CRF. F is the original feature maps of the CNN network. E-CRF utilizes pairwise module ψ_p^f and auxiliary superpixel-based module ψ_s^f on F to obtain refined feature maps F^p and F^s respectively. Then F , F^p and F^s are fused as F^* to further segment the image.

Considering the inherent drawback of CNN networks mentioned before, delving into the relationship between raw pixels becomes a potential alternative to eliminate the BCWC problem, and Conditional Random Field (CRF) (Chen et al., 2014) stands out. It is generally known that pixels of the same object tend to share similar characteristics in the local area. Intuitively, CRF utilizes the local consistency between original image pixels to refine the boundary segmentation results with the help of inner pixels of the same object. CRF makes some boundary pixels that are misclassified by the CNN network quite easy to be recognized correctly. But these CRF-based methods (Chen et al., 2014; Zhen et al., 2020a) only adopt CRF as an offline post-processing module, we call it *Vanilla-CRF*, to refine the final segmentation results. They are incapable of relieving BCWC problem as CRF and the CNN network are treated as two totally separate modules.

Based on Chen et al. (2014; 2017a), Lin et al. (2015); Arnab et al. (2016); Zheng et al. (2015) go a step further to unify the segmentation model and CRF in a single pipeline for end-to-end training. We call it *Joint-CRF* for simplicity. Same as *Vanilla-CRF*, *Joint-CRF* inclines to rectify those misclassified boundary pixels via increasing the prediction score of the associated category, which means it still operates on the *object class probabilities*. But it can alleviate the BCWC problem to some extent as the probability score refined by CRF directly involves in the model backpropagation. Afterwards, the disturbing gradients caused by those pixels will be relieved, which will promote the class representation learning. However, as shown in Fig 3, the effectiveness of Joint-CRF is restricted as it only optimizes the scale of the gradient and lacks the ability to optimize class representations effectively due to the defective design. More theoretical analysis can be found in Sec. 3.3.

To overcome the aforementioned drawbacks, in this paper, we present a novel approach named *Embedded CRF (E-CRF)* to address the BCWC problem more effectively. The superiority of E-CRF lies in two main aspects. On the one hand, by fusing CRF mechanism into the segmentation model, E-CRF utilizes the local consistency among original image pixels to guide the message passing of high-level features. Each pixel pair that comes from the same object tends to obtain higher message passing weights. Therefore, the feature representation of the boundary pixels can be purified by the corresponding inner pixels from the same object. In turn, those pixels will further contribute to the discriminative class representation learning. On the other hand, it extends the fashion of optimizing class weights from one perspective (*i.e.*, scale) to two (*i.e.*, scale and direction) during

¹These methods improve boundary segemetation and may have effect on class weights. But they are not explicit and lack theoretical analysis. We show great benifit of explicitly considering BCWC issue. See A.4.1.

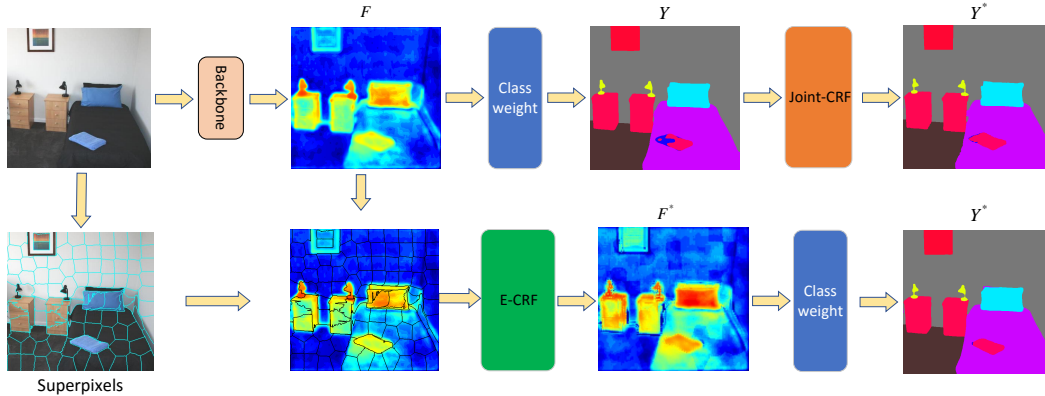


Figure 2: Illustration of Joint-CRF and E-CRF. The first row is the simplified structure of Joint-CRF, which unifies the CNN network and CRF in a single pipeline for end-to-end training. However, CRF only serves as a post-processing module. The second row is the overview of our E-CRF, which fuses CRF into CNN network as an organic whole to eliminate BCWC problem.

backpropagation. In Sec. 3.3, we prove theoretically that E-CRF outperforms other CRF-based methods on eliminating the BCWC problem by optimizing both direction and scale of the disturbing gradient of class weights. However, during this process, the noise information can also have a direct influence on the class weights (likely to hinder the optimization for the BCWC problem). In addition, E-CRF adopts superpixel (Ren & Malik, 2003) as an auxiliary and leverage its local prior to suppress the noise and further strengthen the reliability of the message passing to the boundary pixels. Superpixel groups adjacent pixels that share similar characteristics to form a block. It is prone to achieve clear and smooth boundaries and increases the potential for higher segmentation performance. In E-CRF, we average the deep feature representation of all inner pixels in the same superpixel block and then add this local object prior to each pixel back to enhance the representation of boundary pixels.

In this work, we explicitly propose the BCWC problem in semantic segmentation and an effective approach to alleviate it. We conduct extensive experiments on three challenging semantic segmentation benchmarks, *i.e.*, ADE20K (Zhou et al., 2017), Cityscapes (Cordts et al., 2016), and Pascal Context (Mottaghi et al., 2014), and yield impressive results. For example, E-CRF outperforms baselines (DeeplabV3+ (Chen et al., 2018a) with ResNet-101 (He et al., 2016)) by **1.42%** mIoU on ADE20K and **0.92%** mIoU on Cityscapes in single scale. In addition, we make an exhaustive theoretical analysis in Sec. 3.3 to prove the effectiveness of E-CRF. Code is available at <https://github.com/JiePKU/E-CRF>.

2 RELATED WORK

Semantic Segmentation. Fully convolutional network (FCN) (Long et al., 2015) based methods have made great progress in semantic segmentation by leveraging the powerful convolutional features of classification networks (He et al., 2016; Huang et al., 2017) pre-trained on large-scale data (Rusakovsky et al., 2015). There are several model variants proposed to enhance contextual aggregation. For example, DeeplabV2 (Chen et al., 2017a) and DeeplabV3 (Chen et al., 2017b) take advantage of the astrous spatial pyramid pooling (ASPP) to embed contextual information, which consists of parallel dilated convolutions with different dilated rates to broaden the receptive field. Inspired by the encoder-decoder structures (Ronneberger et al., 2015; Ding et al., 2018), DeeplabV3+ (Chen et al., 2018a) adds a decoder upon DeeplabV3 to refine the segmentation results especially along object boundaries. With the success of self-attention mechanism in natural language processing, Non-local (Wang et al., 2018) first adopts self-attention mechanism as a module for computer vision tasks, such as video classification, object detection and instance segmentation. A²Net (Chen et al., 2018b) proposes the double attention block to distribute and gather informative global features from the entire spatio-temporal space of the images.

Conditional Random Fields. Fully connected CRFs have been used for semantic image labeling in (Payot & Todorovic, 2010; Toyoda & Hasegawa, 2008), but inference complexity in fully connected models has restricted their application to sets of hundreds of image regions or fewer. To address this issue, densely connected pairwise potentials (Krähenbühl & Koltun, 2011) facilitate interactions

between all pairs of image pixels based on a mean field approximation to the CRF distribution. Chen et al. (2014) show further improvements by post-processing the results of a CNN with a CRF. Subsequent works (Lin et al., 2015; Arnab et al., 2016; Zheng et al., 2015) have taken this idea further by incorporating a CRF as layers within a deep network and then learning parameters of both the CRF and CNN together via backpropagation. In terms of enhancements to conventional CRF models, Ladický et al. (2010) propose using an off-the-shelf object detector to provide additional cues for semantic segmentation.

Superpixel. Superpixel (Ren & Malik, 2003) is pixels with similar characteristics that are grouped together to form a large block. Since its introduction in 2003, there have been many mature algorithms (Achanta et al., 2012; Weikersdorfer et al., 2013; Van den Bergh et al., 2012). Owing to their representational and computational efficiency, superpixels are widely-used in computer vision algorithms such as target detection (Shu et al., 2013; Yan et al., 2015), semantic segmentation (Gould et al., 2008; Sharma et al., 2014; Gadde et al., 2016), and saliency estimation (He et al., 2015; Perazzi et al., 2012). Yan et al. (2015) convert object detection problem into superpixel labeling problem and conducts an energy function considering appearance, spatial context and numbers of labels. Gadde et al. (2016) use superpixels to change how information is stored in the higher level of a CNN. In (He et al., 2015), superpixels are taken as input and contextual information is recovered among superpixels, which enables large context to be involved in analysis.

We give a detailed discussion about the difference between E-CRF and three highly related works including PCGrad (Yu et al., 2020b), OCNet (Yuan & Wang, 2018), and SegFix (Yuan et al., 2020b) in Appendix A.5.

3 METHOD

3.1 REVISITING CONDITIONAL RANDOM FIELD (CRF)

CRF is a typical discriminative model suitable for prediction tasks where contextual information or the state of the neighbors affects the current prediction. Nowadays, it is widely adopted in the semantic segmentation field (Krähenbühl & Koltun, 2011; Chen et al., 2014). CRF utilizes the correlation between original image pixels to refine the segmentation results by modeling this problem as the maximum a posteriori (MAP) inference in a conditional random field (CRF), defined over original image pixels. In practice, the most common way is to approximate CRF as a message passing procedure among pixels and it can be formulated as:

$$Y_i^* = \frac{1}{Z_i} (\psi_u(i) + \sum_{j \neq i}^G \psi_p(i, j) Y_j), \quad (1)$$

where Y_i and Y_i^* are defined as the classification scores of CNN model and CRF respectively for pixel i , Z_i is the normalization factor known as the partition function, and $\psi_u(i)$ is a unary function which often adopts Y_i as the default value. G is the associated pixel set with pixel i . For example, DenseCRF (Krähenbühl & Koltun, 2011) takes all other pixels except pixel i itself as the set G . Moreover, the pairwise function $\psi_p(i, j)$ is defined to measure the message passing weight from pixel j to pixel i . It is formulated as:

$$\psi_p(i, j) = \mu(i, j) \underbrace{\sum_{m=1}^M \omega^{(m)} k^{(m)}(\mathbf{f}_i, \mathbf{f}_j)}_{k(\mathbf{f}_i, \mathbf{f}_j)}, \quad (2)$$

where $\mu(i, j)$ is a label compatibility function that introduces the co-occurrent probability for a specific label pair assignment at pixel i and j , while $k(\mathbf{f}_i, \mathbf{f}_j)$ is a set of hand-designed Gaussian kernels, \mathbf{f}_i and \mathbf{f}_j are feature vectors of pixel i and j in any arbitrary feature space, such as RGB images. $\omega^{(m)}$ is the corresponding linear combination weight for each Gaussian kernel. When dealing with multi-class image segmentation, $M=2$ is a common setting. Then, $k(\mathbf{f}_i, \mathbf{f}_j)$ is carefully designed as contrast-sensitive two-kernel potentials, defined in terms of color vectors (I_i, I_j) and

position coordinates (p_i, p_j) for pixel i and j respectively:

$$k(\mathbf{f}_i, \mathbf{f}_j) = \underbrace{w^{(1)} \exp\left(-\frac{|p_i - p_j|^2}{2\theta_\alpha^2} - \frac{|I_i - I_j|^2}{2\theta_\beta^2}\right)}_{\text{appearance kernel}} + \underbrace{w^{(2)} \exp\left(-\frac{|p_i - p_j|^2}{2\theta_\gamma^2}\right)}_{\text{smoothness kernel}}. \quad (3)$$

The appearance kernel is inspired by the observation that nearby pixels with similar colors are more likely to share the same class. θ_α and θ_β are scale factors to control the degree of these two elements, *i.e.*, similarity and distance between two pixels. Apart from this, the smoothness kernel further removes the influence of some small isolated regions (Krähenbühl & Koltun, 2011) and θ_γ is the associated scale factor. Notably, all these parameters are learnable during the model training.

Unfortunately, current CRF-based methods (Chen et al., 2014; 2017a; Lin et al., 2015; Liu et al., 2015) for semantic segmentation always adopt CRF as a post-processing module. For example, Vanilla-CRF (Chen et al., 2014; 2017a) utilizes CRF to refine segmentation scores offline, which has no impacts on BCWC since the CNN network and CRF are treated as two separate modules. Joint-CRF (Lin et al., 2015; Liu et al., 2015; Lin et al., 2016) works in a similar way although CRF involves in the backpropagation of CNN networks, restricting its ability to relieve BCWC.

3.2 EMBEDDED CRF

To solve the BCWC problem in a more intrinsical way, we propose a novel method named *Embedded CRF* (E-CRF) to tackle the tough problem via fusing the CRF mechanism into the CNN network as an organic whole for more effective end-to-end training. An overview of E-CRF can be found in Fig 2 and we formulate its core function based on Eq (1) as:

$$F_i^* = \frac{1}{Z_i} \left\{ \psi_u^f(i) + \sum_{j \neq i}^G \psi_p^f(i, j) F_j + F_i^S \right\}. \quad (4)$$

Specifically, the first two terms are analogous to Eq (1) but we perform CRF mechanism on the high-level features. F_i stands for the original output of feature extractors for pixel i , $\psi_u^f(i)$ and $\psi_p^f(i, j)$ play the same role as they do in Eq (1). $\psi_u^f(i)$ takes F_i as the default value. In addition, we reformulate $\psi_p^f(i, j)$ to perform message passing between pixel pairs in the high-level feature:

$$\psi_p^f(i, j) = \mu^f(i, j) k(\mathbf{f}_i, \mathbf{f}_j). \quad (5)$$

It is worth noting that $k(\mathbf{f}_i, \mathbf{f}_j)$ is no longer hand-designed Gaussian kernels as it is in Eq (1) but simple convolution operators instead to make the whole model more flexible for end-to-end training and optimization. Experiments in Sec. 4 prove this modification is a more suitable choice:

$$k(\mathbf{f}_i, \mathbf{f}_j) = \mathbf{f}_i \cdot \mathbf{f}_j = \text{conv}([I_i, p_i]) \cdot \text{conv}([I_j, p_j]), \quad (6)$$

where $[x, y]$ denotes the concatenation operator. Different from Eq (3), we normalize the input image I into the range $[0, 1]$ to eliminate the scale variance between pixels and we replace original absolute position coordinates p with *cosine* position embeddings (Vaswani et al., 2017) to make it more compatible with CNN networks. E-CRF encodes the appearance and position of pixels into more discriminative tokens via the flexible convolution operation, then the dot product is adopted to measure the similarity between pixel pairs. As indicated in Eq (6), E-CRF intends to make nearby pixel pairs that share same appearance to achieve higher $k(\mathbf{f}_i, \mathbf{f}_j)$. Its intention is the same as Eq (3). Correspondingly, we also adjust $\mu^f(i, j)$ as the feature compatibility to measure the co-occurrent probability of F_i and F_j :

$$\mu^f(i, j) = \text{sigmoid}(\text{conv}[F_i, F_j]). \quad (7)$$

Another component in Eq (4) is F_i^S . It relies on the superpixel algorithm (Ren & Malik, 2003; Weikersdorfer et al., 2013; Van den Bergh et al., 2012; Gadde et al., 2016) to divide the whole image I into several non-overlapping blocks. Pixels in the same superpixel block tend to share the same characteristics. Thus, we adopt this local object prior to achieve the more effective message passing between pixels in the high-level feature space. Concretely, we design F_i^S as:

$$F_i^S = \sum_l^Q \psi_s^f(l) F_l = \sum_l^Q \frac{1}{n} F_l \quad (8)$$

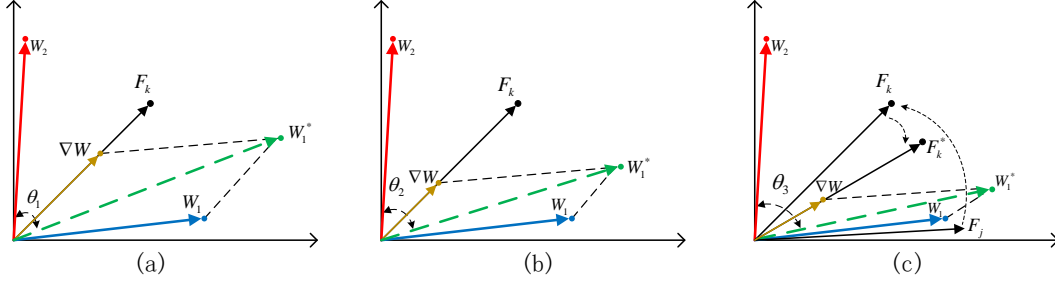


Figure 3: Different optimization effects for baseline, Joint-CRF and E-CRF. W_1 and W_2 are two class weight vectors that share adjacent pixels. ∇W is the gradient variation for W_1 and W_1^* is the new class weight after gradient descent. F_k is a sample boundary pixel whose ground-truth label keeps consistent with W_1 but contains confusing features from both sides. θ measures the distance between W_2 and W_1^* . **(a)** ∇W tends to push W_1 towards W_2 due to the confusing features from both classes. **(b)** Joint-CRF eases the disturbing gradients and reduces the scale of ∇W . Obviously, θ_2 is larger than θ_1 . **(c)** E-CRF aims to enhance the feature representation of F_k via the inner pixels like F_j from the same object. It adjusts both scale and direction of ∇W to make $\theta_3 > \theta_2 > \theta_1$.

Q is the associated superpixel block that contains pixel i and $\psi_s^f(l)$ devotes the re-weighting factor for the deep features of pixel l in Q . We adopt $\psi_s^f(l) = \frac{1}{n}$ and n is the total number of pixels in Q . F_i^S serves as a supplement in Eq (4) to add the local object prior to each pixel back, which increases the reliability of message passing in E-CRF. What's more, superpixel (Gould et al., 2008; Sharma et al., 2014; Gadde et al., 2016) always tends to generate clearer and smoother boundary segmentation results than traditional CNN networks or CRFs do, which also increases the potential for more accurate segmentation results. Detailed experiments can be found in Sec. 4.

3.3 HOW E-CRF RELIEVES BCWC

In this section, without loss of generality, we take multi-class segmentation problem as an example to dive into the principle of E-CRF from the perspective of gradient descent. Suppose F_k is the feature vector of a foreground boundary pixel k whose class label is $c \in [0, n - 1]$ and its prediction probability is P_k^c . Then, considering the label y_k is one-hot form, the typical cross-entropy loss L_k can be defined as:

$$L_k = - \sum_{i=0}^{i < n} y_k^i \ln P_k^i = - \ln P_k^c, \quad (9)$$

$$P_k^c = \text{softmax}(Y_k^c) = \frac{e^{Y_k^c}}{(\sum_{m \neq c} e^{Y_k^m}) + e^{Y_k^c}}, \quad \text{and} \quad Y_k^c = W_c^T \cdot F_k, \quad (10)$$

where W_c is the class weight of c -th category. Y_k^m is calculated by other class weights and unrelated with W_c and Y_k^c . Below the gradient variation ∇W_c can be formulated as:

$$\nabla W_c = \frac{\partial L_k}{\partial W_c} = \frac{\partial L_k}{\partial P_k^c} \cdot \frac{\partial P_k^c}{\partial Y_k^c} \cdot \frac{\partial Y_k^c}{\partial W_c} \quad (11)$$

Through Eq (9), Eq (10) and Eq (11), class weight in the next iteration will be updated ²:

$$W_c^* = W_c - \nabla W_c = W_c + (1 - P_k^c) \cdot F_k \quad (12)$$

As shown in Eq (12), the direction of the gradient descent keeps the same as F_k while the magnitude of the gradient is decided by P_k^c . *What happens if we integrate the CRF into the segmentation pipeline?* As we have discussed in Sec. 1, Vanilla-CRF has nothing to do with the optimization process of CNN networks, while if we adopt Joint-CRF, ∇W_c can be reformulated as:

$$-\nabla W_c = (1 - \hat{P}_k^c) \cdot F_k = \underbrace{\left(1 - \frac{1}{Z_k} \left(\sum_{j \in G} w_j P_j^c + P_k^c\right)\right)}_{\text{scale}} \cdot F_k \quad (13)$$

²The detailed derivation process can be found in our *Appendix A.1*.

where \hat{P}_k^c is the refined score by CRF, w_j is the message passing weight from pixel j to pixel k and P_j^c is the original score of pixel j . In general, boundary pixel k is hard to classify correctly due to the confusing features from both sides. Thus the original probability P_k^c is always small. In contrast, other inner pixels of the same object are easy to recognize and tend to achieve a higher probability. Consequently, \hat{P}_k^c is usually larger than P_k^c and disturbing gradients caused by boundary pixel will be relieved to some extent, which makes inter-class distance further as shown in Fig 3(b). However, Eq (13) only adjusts the scale of the gradient descent while the direction still keeps the same as F_k , which weakens its effects for better representation learning. When it comes to our proposed E-CRF, ∇W_c can be further defined as:

$$-\nabla W_c = (1 - P_k^{c*}) \cdot F_k^* = \underbrace{(1 - P_k^{c*})}_{scale} \cdot \underbrace{\frac{1}{Z_k} \left(\sum_{j \in G} w_j F_j + F_k \right)}_{direction} \quad (14)$$

$$P_k^{c*} = softmax\left(\sum_{j \in G} w_j Y_j^c + Y_k^c\right) \quad (15)$$

where F_k^* is the refined feature representations by E-CRF, and P_k^{c*} is the refined score which is analogous to \hat{P}_k^c in Eq (13). Comparing with Joint-CRF, it is clear that E-CRF not only changes the scale of the gradient descent but also adjusts its optimization direction. The optimization process is directly applied to the class weight matrix (in the final layer), which opens up room for more discriminative class weights. In other words, we can adjust the class weight from both the scale and direction to make the class weights more discriminative to decrease the class weights similarity (or class weights confusion). As depicted in Fig 3(c), assume W_1 is the class weight vector that a pixel belongs to, while W_2 is the other one which has a higher co-occurrent probability with W_1 in the same image. E-CRF designs an effective message passing procedure to purify the feature representation of boundary pixels assisted by inner pixels from the same object (F_j in Fig 3(c)). In this way, it relieves the influence of disturbing gradients and makes the inter-class distance between $W_1(W_1^*)$ and W_2 further, which means more discriminative feature representations.

4 EXPERIMENT

4.1 IMPLEMENTATION DETAILS

We follow the previous works (Chen et al., 2014; He et al., 2019b; Chen et al., 2018a) and perform experiments on three challenging semantic segmentation benchmarks, *i.e.*, ADE20K (Zhou et al., 2017), Cityscapes (Cordts et al., 2016) and Pascal Context (Mottaghi et al., 2014). Due to the space limit, a detailed description of these three datasets can be found in our *Appendix A*. We adopt DeeplabV3+ (Chen et al., 2018a) with ResNet (He et al., 2016) pretrained on ImageNet (Russakovsky et al., 2015) as our baseline to implement E-CRF. The detailed information follows standard settings in (Chen et al., 2014; 2018a) and we add it into our *Appendix A*. Specially, we employ SLIC (Achanta et al., 2012), a common superpixel segmentation algorithm, to divide each image of ADE20K, Cityscapes and Pascal Context into 200, 600, and 200 blocks respectively. Note that the superpixel is generated offline. To verify the effectiveness of our approach for semantic segmentation, we adopt two common metrics in our experiments, *i.e.*, class-wise mIoU to measure the overall segmentation performance and 1-pixel boundary F-score (Takikawa et al., 2019; Tan et al., 2023) to measure the boundary segmentation performance.

4.2 ABLATION STUDY

4.2.1 COMPARISONS WITH RELATED METHODS

As shown in Table 1, we compare our proposed E-CRF with other traditional CRF-based methods, *i.e.*, Vanilla-CRF and Joint-CRF. First of all, it is clear that all the CRF-based methods outperform the baseline model by a large margin, which well verifies the main claim in (Chen et al., 2014; 2017a; Lin et al., 2015; Liu et al., 2015; Lin et al., 2016) that CRF is beneficial to boundary segmentation (F-score). What’s more, E-CRF achieves the best result among all those methods, which surpasses the baseline model with up to **1.48%** mIoU and **2.20%** F-score improvements. E-CRF fuses the CRF mechanism into the CNN network as an organic whole. It relieves the disturbing gradients caused

Table 1: Comparisons with baseline, Vanilla-CRF and Joint-CRF on ADE20K *val* dataset. ³It stands for DeeplabV3+ followed by DenseCRF. ⁴An end-to-end manner of Vanilla-CRF, similar to (Zheng et al., 2015).

Method	ResNet-50		ResNet-101	
	F-score (%)	mIoU (%)	F-score (%)	mIoU (%)
DeeplabV3+	14.25	42.72	16.15	44.60
Vanilla-CRF ³	16.26	43.18 (+0.46)	17.89	45.14 (+0.54)
Joint-CRF ⁴	16.32	43.69 (+0.96)	18.03	45.61 (+1.01)
E-CRF (Ours)	16.45	44.20 (+1.48)	18.32	46.02 (+1.42)

by the BCWC problem and adjusts the feature representations to boost the overall segmentation performance and the boundary segmentation. Fig 1(a) also proves that E-CRF can decrease the inter-class similarity consistently which results in more discriminative feature representations. Experiments on Cityscapes dataset can be found in our *Appendix A*.

4.2.2 ABLATION ON MESSAGE PASSING STRATEGIES

As we have discussed in Sec. 3.2, two message passing components, *i.e.*, pairwise module ψ_p^f and superpixel-based module ψ_s^f , play vital roles in our proposed E-CRF. Table 2 shows that ψ_p^f and ψ_s^f can boost the overall segmentation performance on ADE20K *val* dataset with up to **1.19%** mIoU and **1.25%** mIoU gains when integrated into the baseline model respectively. Moreover, if we fuse them as a whole into E-CRF, they can further promote the segmentation performance by up to **1.48%** mIoU improvements. We also compare with Non-local (Wang et al., 2018), another famous attention-based message passing method, into our experiments for comprehensive comparisons even though it actually has different design concepts from ours. Unfortunately, we find that although Non-local achieves improvements over the baseline, it is still inferior to our E-CRF.

Table 2: Comparisons between message passing strategies, and ablation studies for different message passing components in E-CRF, pairwise ψ_p^f and auxiliary superpixel-based ψ_s^f .

Method	ψ_p^f	ψ_s^f	mIoU(%)	
			ResNet-50	ResNet-101
DeeplabV3+ + Non-local			42.72	44.60
			43.52 (\uparrow 0.80)	45.34 (\uparrow 0.74)
E-CRF	\checkmark		43.91 (\uparrow 1.19)	45.47 (\uparrow 0.87)
		\checkmark	43.83 (\uparrow 1.11)	45.85 (\uparrow 1.25)
	\checkmark	\checkmark	44.20 (\uparrow 1.48)	46.02 (\uparrow 1.42)

4.2.3 ABLATION OF SUPERPIXEL NUMBERS

We follow standard settings in our paper and take DeeplabV3+ based on ResNet-50 as the baseline model to present the performance of E-CRF under different superpixel numbers. Detailed comparisons on ADE20K dataset are reported in Table 3 and **SP** denotes **SuperPixel**. As shown in Table 3, different numbers of superpixels indeed affect the performance of E-CRF. Intuitively, when the number of superpixels is 200, E-CRF acquires the best performance as it achieves a better trade-off between the superpixel purity and the long-range dependency. Moreover, it is worth noting that when the pairwise message passing strategy (*i.e.*, ψ_p^f) is also adopted in E-CRF, it becomes more robust to the different numbers of superpixels that may introduce noise, as our adaptive message passing mechanism (including ψ_p^f and ψ_s^f) can be compatible with the variance.

Table 3: Comparisons with different superpixel numbers on ADE20K *val* dataset.

SP num	mIoU w\ ψ_p^f (%)	mIoU w\ ψ_s^f (%)
No	43.91	42.72
100	44.02	43.43
200	44.20	43.83
300	44.13	43.56
400	43.96	43.22

More ablation studies including comparison of different boundary refinement and computational cost are presented in Appendix A.4.

Table 4: Comparisons with other state-of-the-art methods on ADE20K *val* dataset, Cityscapes *val* and *test*, and Pascal Context *val* dataset.

Method	backbone	mIoU(%)			
		ADE- <i>val</i>	City- <i>val</i>	City- <i>test</i>	Pas-Con
CCNet (Huang et al., 2019)	ResNet101	45.22	81.3	81.9	-
ANL (Zhu et al., 2019)	ResNet101	45.24	-	-	52.8
GFFNet (Li et al., 2020c)	ResNet101	45.33	81.8	82.3	54.2
APCNet (He et al., 2019b)	ResNet101	45.38	-	-	54.7
DMNet (He et al., 2019a)	ResNet101	45.50	-	-	54.4
SpyGR (Li et al., 2020a)	ResNet101	-	80.5	81.6	52.8
RecoNet (Chen et al., 2020)	ResNet101	45.54	81.6	82.3	54.8
SPNet (Hou et al., 2020)	ResNet101	45.60	-	-	54.5
DNL (Yin et al., 2020)	ResNet101	45.82	-	-	55.3
RANet (Shen et al., 2020)	ResNet101	-	81.9	82.4	54.9
ACNet (Fu et al., 2019)	ResNet101	45.90	82.0	82.3	54.1
HANet (Choi et al., 2020)	ResNet101	-	82.05	82.1	-
RPCNet (Zhen et al., 2020b)	ResNet101	-	82.1	81.8	-
CaCNet (Liu et al., 2020)	ResNet101	46.12	-	-	55.4
CPNet (Yu et al., 2020a)	ResNet101	46.27	-	-	53.9
STLNet (Zhu et al., 2021)	ResNet101	46.48	82.3	82.3	55.6
E-CRF (Ours)	ResNet101	46.83	82.74	82.5	56.1

4.3 COMPARISONS WITH SOTA METHODS

In this research, we mainly focus on the *Boundary-caused Class Weight Confusion (BCWC)* in CNN models. Hence, in this section, we choose CNN-based methods for fair comparisons.⁵

ADE20K. We first compare our E-CRF (ResNet101 as backbone) with existing methods on the ADE20K *val* set. We follow standard settings in (Huang et al., 2019; Yuan et al., 2020a; Zhu et al., 2021) to adopt multi-scale testing and left-right flipping strategies. Results are presented in Table 4. It is shown that E-CRF outperforms existing approaches. Segmentation visualization is presented in our *Appendix*

Cityscapes. To verify the generalization of our method, we perform detailed comparisons with other SOTA methods on Cityscapes *val* and *test* set. Multi-scale testing and left-right flipping strategies are also adopted. The results with ResNet101 as backbone are reported in Table 4. Remarkably, our algorithm achieves **82.74%** mIoU in val set and outperforms previous methods by a large margin.

Pascal Context. To further verify the generalization of E-CRF (ResNet101 as backbone), we compare our method with other SOTA method on Pascal Context dataset as shown in Table 4. We adopt multi-scale testing and left-right flipping strategies as well. The result suggests the superiority of our method.

5 CONCLUSION AND FUTURE WORKS

In this paper, we focus on the particularity of class weights in semantic segmentation and explicitly consider an important issue, named as *Boundary-caused Class Weights Confusion (BCWC)*. We dive deep into it and propose a novel method, *E-CRF*, via combining CNN network with CRF as an organic whole to alleviate BCWC from two aspects (*i.e.*, scale and direction). In addition, we make an exhaustive theoretical analysis to prove the effectiveness of E-CRF. Eventually, our proposed method achieves new results on ADE20K, Cityscapes, and Pascal Context datasets.

There are two important directions for future research. In this work, we use SLIC, a common cluster-based algorithm for fast implementation. There exist many other superpixel algorithms such as graphical-based (Felzenszwalb & Huttenlocher, 2004) and CNN-based (Jampani et al., 2018) that may give better boundary results for objects. Therefore how these different methods influence the performance in our framework is interesting. Besides, We find that transformer-based networks suffer from BCWC issue as well and make a preliminary exploration. More works are expected to focus on this issue.

⁵We also conduct experiments based on SegFormer (Xie et al., 2021) to make a preliminary exploration in our Appendix B as we found that BCWC issue also exists in transformer-based models.

ACKNOWLEDGMENTS

We thank the anonymous reviewers for their constructive comments. We also sincerely thank Tiancai Wang for useful discussion. This work is supported by the NSFC Grants no. 61972008.

REFERENCES

- Radhakrishna Achanta, Appu Shaji, Kevin Smith, Aurelien Lucchi, Pascal Fua, and Sabine Süsstrunk. Slic superpixels compared to state-of-the-art superpixel methods. *IEEE transactions on pattern analysis and machine intelligence*, 34(11):2274–2282, 2012.
- Anurag Arnab, Sadeep Jayasumana, Shuai Zheng, and Philip HS Torr. Higher order conditional random fields in deep neural networks. In *Computer Vision—ECCV 2016: 14th European Conference, Amsterdam, The Netherlands, October 11–14, 2016, Proceedings, Part II 14*, pp. 524–540. Springer, 2016.
- Liang-Chieh Chen, George Papandreou, Iasonas Kokkinos, Kevin Murphy, and Alan L Yuille. Semantic image segmentation with deep convolutional nets and fully connected crfs. *arXiv preprint arXiv:1412.7062*, 2014.
- Liang-Chieh Chen, George Papandreou, Iasonas Kokkinos, Kevin Murphy, and Alan L Yuille. Deeplab: Semantic image segmentation with deep convolutional nets, atrous convolution, and fully connected crfs. *IEEE transactions on pattern analysis and machine intelligence*, 40(4):834–848, 2017a.
- Liang-Chieh Chen, George Papandreou, Florian Schroff, and Hartwig Adam. Rethinking atrous convolution for semantic image segmentation. *arXiv preprint arXiv:1706.05587*, 2017b.
- Liang-Chieh Chen, Yukun Zhu, George Papandreou, Florian Schroff, and Hartwig Adam. Encoder-decoder with atrous separable convolution for semantic image segmentation. In *Proceedings of the European conference on computer vision (ECCV)*, pp. 801–818, 2018a.
- Wanli Chen, Xinge Zhu, Ruoqi Sun, Junjun He, Ruiyu Li, Xiaoyong Shen, and Bei Yu. Tensor low-rank reconstruction for semantic segmentation. In Andrea Vedaldi, Horst Bischof, Thomas Brox, and Jan-Michael Frahm (eds.), *Computer Vision – ECCV 2020*, pp. 52–69, Cham, 2020. Springer International Publishing. ISBN 978-3-030-58520-4.
- Yunpeng Chen, Yannis Kalantidis, Jianshu Li, Shuicheng Yan, and Jiashi Feng. A²-nets: Double attention networks. In S. Bengio, H. Wallach, H. Larochelle, K. Grauman, N. Cesa-Bianchi, and R. Garnett (eds.), *Advances in Neural Information Processing Systems*, volume 31. Curran Associates, Inc., 2018b.
- Sungha Choi, Joanne T. Kim, and Jaegul Choo. Cars can’t fly up in the sky: Improving urban-scene segmentation via height-driven attention networks. In *IEEE/CVF Conference on Computer Vision and Pattern Recognition (CVPR)*, June 2020.
- Xiangxiang Chu, Zhi Tian, Yuqing Wang, Bo Zhang, Haibing Ren, Xiaolin Wei, Huaxia Xia, and Chunhua Shen. Twins: Revisiting the design of spatial attention in vision transformers. *Advances in Neural Information Processing Systems*, 34, 2021.
- Marius Cordts, Mohamed Omran, Sebastian Ramos, Timo Rehfeld, Markus Enzweiler, Rodrigo Benenson, Uwe Franke, Stefan Roth, and Bernt Schiele. The cityscapes dataset for semantic urban scene understanding. In *Proc. of the IEEE Conference on Computer Vision and Pattern Recognition (CVPR)*, 2016.
- Henghui Ding, Xudong Jiang, Bing Shuai, Ai Qun Liu, and Gang Wang. Context contrasted feature and gated multi-scale aggregation for scene segmentation. In *Proceedings of the IEEE Conference on Computer Vision and Pattern Recognition*, pp. 2393–2402, 2018.
- Henghui Ding, Xudong Jiang, Ai Qun Liu, Nadia Magnenat Thalmann, and Gang Wang. Boundary-aware feature propagation for scene segmentation. In *Proceedings of the IEEE/CVF International Conference on Computer Vision*, pp. 6819–6829, 2019.

- Pedro F Felzenszwalb and Daniel P Huttenlocher. Efficient graph-based image segmentation. *International journal of computer vision*, 59:167–181, 2004.
- Jun Fu, Jing Liu, Yuhang Wang, Yong Li, Yongjun Bao, Jinhui Tang, and Hanqing Lu. Adaptive context network for scene parsing. In *Proceedings of the IEEE/CVF International Conference on Computer Vision*, pp. 6748–6757, 2019.
- Raghudeep Gadde, Varun Jampani, Martin Kiefel, Daniel Kappler, and Peter V Gehler. Superpixel convolutional networks using bilateral inceptions. In *European conference on computer vision*, pp. 597–613. Springer, 2016.
- Stephen Gould, Jim Rodgers, David Cohen, Gal Elidan, and Daphne Koller. Multi-class segmentation with relative location prior. *International Journal of Computer Vision*, 80(3):300–316, 2008.
- Junjun He, Zhongying Deng, and Yu Qiao. Dynamic multi-scale filters for semantic segmentation. In *Proceedings of the IEEE/CVF International Conference on Computer Vision*, pp. 3562–3572, 2019a.
- Junjun He, Zhongying Deng, Lei Zhou, Yali Wang, and Yu Qiao. Adaptive pyramid context network for semantic segmentation. In *Proceedings of the IEEE/CVF Conference on Computer Vision and Pattern Recognition*, pp. 7519–7528, 2019b.
- Kaiming He, Xiangyu Zhang, Shaoqing Ren, and Jian Sun. Deep residual learning for image recognition. In *Proceedings of the IEEE conference on computer vision and pattern recognition*, pp. 770–778, 2016.
- Shengfeng He, Rynson WH Lau, Wenxi Liu, Zhe Huang, and Qingxiong Yang. Supercnn: A superpixelwise convolutional neural network for salient object detection. *International journal of computer vision*, 115(3):330–344, 2015.
- Qibin Hou, Li Zhang, Ming-Ming Cheng, and Jiashi Feng. Strip pooling: Rethinking spatial pooling for scene parsing. In *Proceedings of the IEEE/CVF Conference on Computer Vision and Pattern Recognition*, pp. 4003–4012, 2020.
- Gao Huang, Zhuang Liu, Laurens Van Der Maaten, and Kilian Q Weinberger. Densely connected convolutional networks. In *Proceedings of the IEEE conference on computer vision and pattern recognition*, pp. 4700–4708, 2017.
- Zilong Huang, Xinggang Wang, Lichao Huang, Chang Huang, Yunchao Wei, and Wenyu Liu. Ccnet: Criss-cross attention for semantic segmentation. In *Proceedings of the IEEE/CVF International Conference on Computer Vision*, pp. 603–612, 2019.
- Varun Jampani, Deqing Sun, Ming-Yu Liu, Ming-Hsuan Yang, and Jan Kautz. Superpixel sampling networks. In *Proceedings of the European Conference on Computer Vision (ECCV)*, pp. 352–368, 2018.
- Philipp Krähenbühl and Vladlen Koltun. Efficient inference in fully connected crfs with gaussian edge potentials. *Advances in neural information processing systems*, 24:109–117, 2011.
- L'ubor Ladický, Paul Sturges, Karteek Alahari, Chris Russell, and Philip H. S. Torr. What, where and how many? combining object detectors and crfs. In Kostas Daniilidis, Petros Maragos, and Nikos Paragios (eds.), *Computer Vision – ECCV 2010*, pp. 424–437, Berlin, Heidelberg, 2010. Springer Berlin Heidelberg.
- Xia Li, Yibo Yang, Qijie Zhao, Tiancheng Shen, Zhouchen Lin, and Hong Liu. Spatial pyramid based graph reasoning for semantic segmentation. In *Proceedings of the IEEE/CVF Conference on Computer Vision and Pattern Recognition*, pp. 8950–8959, 2020a.
- Xiangtai Li, Xia Li, Li Zhang, Guangliang Cheng, Jianping Shi, Zhouchen Lin, Shaohua Tan, and Yunhai Tong. Improving semantic segmentation via decoupled body and edge supervision. In *Computer Vision–ECCV 2020: 16th European Conference, Glasgow, UK, August 23–28, 2020, Proceedings, Part XVII 16*, pp. 435–452. Springer, 2020b.

- Xiangtai Li, Houlong Zhao, Lei Han, Yunhai Tong, Shaohua Tan, and Kuiyuan Yang. Gated fully fusion for semantic segmentation. In *Proceedings of the AAAI Conference on Artificial Intelligence*, pp. 11418–11425, 2020c.
- Guosheng Lin, Chunhua Shen, Ian Reid, and Anton van den Hengel. Deeply learning the messages in message passing inference. *Advances in Neural Information Processing Systems*, 28, 2015.
- Guosheng Lin, Chunhua Shen, Anton Van Den Hengel, and Ian Reid. Efficient piecewise training of deep structured models for semantic segmentation. In *Proceedings of the IEEE conference on computer vision and pattern recognition*, pp. 3194–3203, 2016.
- Jianbo Liu, Junjun He, Yu Qiao, Jimmy S. Ren, and Hongsheng Li. Learning to predict context-adaptive convolution for semantic segmentation. In Andrea Vedaldi, Horst Bischof, Thomas Brox, and Jan-Michael Frahm (eds.), *Computer Vision – ECCV 2020*, pp. 769–786, Cham, 2020. Springer International Publishing. ISBN 978-3-030-58595-2.
- Ze Liu, Yutong Lin, Yue Cao, Han Hu, Yixuan Wei, Zheng Zhang, Stephen Lin, and Baining Guo. Swin transformer: Hierarchical vision transformer using shifted windows. In *Proceedings of the IEEE/CVF international conference on computer vision*, pp. 10012–10022, 2021.
- Ziwei Liu, Xiao Xiao Li, Ping Luo, Chen-Change Loy, and Xiaoou Tang. Semantic image segmentation via deep parsing network. In *Proceedings of the IEEE international conference on computer vision*, pp. 1377–1385, 2015.
- Jonathan Long, Evan Shelhamer, and Trevor Darrell. Fully convolutional networks for semantic segmentation. In *Proceedings of the IEEE conference on computer vision and pattern recognition*, pp. 3431–3440, 2015.
- Roozbeh Mottaghi, Xianjie Chen, Xiaobai Liu, Nam-Gyu Cho, Seong-Whan Lee, Sanja Fidler, Raquel Urtasun, and Alan Yuille. The role of context for object detection and semantic segmentation in the wild. In *Proceedings of the IEEE conference on computer vision and pattern recognition*, pp. 891–898, 2014.
- Nadia Payet and Sinisa Todorovic. $\hat{2}$ -random forest random field. *Advances in Neural Information Processing Systems*, 23, 2010.
- Chao Peng, Tete Xiao, Zeming Li, Yuning Jiang, Xiangyu Zhang, Kai Jia, Gang Yu, and Jian Sun. Megdet: A large mini-batch object detector. In *Proceedings of the IEEE Conference on Computer Vision and Pattern Recognition*, pp. 6181–6189, 2018.
- Federico Perazzi, Philipp Krähenbühl, Yael Pritch, and Alexander Hornung. Saliency filters: Contrast based filtering for salient region detection. In *2012 IEEE conference on computer vision and pattern recognition*, pp. 733–740. IEEE, 2012.
- René Ranftl, Alexey Bochkovskiy, and Vladlen Koltun. Vision transformers for dense prediction. In *Proceedings of the IEEE/CVF International Conference on Computer Vision*, pp. 12179–12188, 2021.
- Xiaofeng Ren and Jitendra Malik. Learning a classification model for segmentation. In *Computer Vision, IEEE International Conference on*, volume 2, pp. 10–10. IEEE Computer Society, 2003.
- Olaf Ronneberger, Philipp Fischer, and Thomas Brox. U-net: Convolutional networks for biomedical image segmentation. In *International Conference on Medical image computing and computer-assisted intervention*, pp. 234–241. Springer, 2015.
- Olga Russakovsky, Jia Deng, Hao Su, Jonathan Krause, Sanjeev Satheesh, Sean Ma, Zhiheng Huang, Andrej Karpathy, Aditya Khosla, Michael Bernstein, et al. Imagenet large scale visual recognition challenge. *International journal of computer vision*, 115(3):211–252, 2015.
- Abhishek Sharma, Oncel Tuzel, and Ming-Yu Liu. Recursive context propagation network for semantic scene labeling. In *NIPS*, volume 1, pp. 2, 2014.

- Dingguo Shen, Yuanfeng Ji, Ping Li, Yi Wang, and Di Lin. Ranet: Region attention network for semantic segmentation. *Advances in Neural Information Processing Systems*, 33:13927–13938, 2020.
- Guang Shu, Afshin Dehghan, and Mubarak Shah. Improving an object detector and extracting regions using superpixels. In *Proceedings of the IEEE Conference on Computer Vision and Pattern Recognition*, pp. 3721–3727, 2013.
- Robin Strudel, Ricardo Garcia, Ivan Laptev, and Cordelia Schmid. Segmenter: Transformer for semantic segmentation. In *Proceedings of the IEEE/CVF International Conference on Computer Vision*, pp. 7262–7272, 2021.
- Towaki Takikawa, David Acuna, Varun Jampani, and Sanja Fidler. Gated-scnn: Gated shape cnns for semantic segmentation. In *Proceedings of the IEEE/CVF international conference on computer vision*, pp. 5229–5238, 2019.
- Haoru Tan, Sitong Wu, and Jimin Pi. Semantic diffusion network for semantic segmentation. *arXiv preprint arXiv:2302.02057*, 2023.
- Takahiro Toyoda and Osamu Hasegawa. Random field model for integration of local information and global information. *IEEE Transactions on Pattern Analysis and Machine Intelligence*, 30(8): 1483–1489, 2008.
- Michael Van den Bergh, Xavier Boix, Gemma Roig, Benjamin de Capitani, and Luc Van Gool. Seeds: Superpixels extracted via energy-driven sampling. In *European conference on computer vision*, pp. 13–26. Springer, 2012.
- Ashish Vaswani, Noam Shazeer, Niki Parmar, Jakob Uszkoreit, Llion Jones, Aidan N Gomez, Łukasz Kaiser, and Illia Polosukhin. Attention is all you need. *Advances in neural information processing systems*, 30, 2017.
- Chi Wang, Yunke Zhang, Miaomiao Cui, Peiran Ren, Yin Yang, Xuansong Xie, Xian-Sheng Hua, Hujun Bao, and Weiwei Xu. Active boundary loss for semantic segmentation. In *Proceedings of the AAAI Conference on Artificial Intelligence*, volume 36, pp. 2397–2405, 2022.
- Xiaolong Wang, Ross Girshick, Abhinav Gupta, and Kaiming He. Non-local neural networks. In *Proceedings of the IEEE conference on computer vision and pattern recognition*, pp. 7794–7803, 2018.
- David Weikersdorfer, Alexander Schick, and Daniel Cremers. Depth-adaptive supervoxels for rgb-d video segmentation. In *2013 IEEE International Conference on Image Processing*, pp. 2708–2712. IEEE, 2013.
- Enze Xie, Wenhai Wang, Zhiding Yu, Anima Anandkumar, Jose M Alvarez, and Ping Luo. Segformer: Simple and efficient design for semantic segmentation with transformers. *Advances in Neural Information Processing Systems*, 34:12077–12090, 2021.
- Junjie Yan, Yinan Yu, Xiangyu Zhu, Zhen Lei, and Stan Z Li. Object detection by labeling superpixels. In *Proceedings of the IEEE Conference on Computer Vision and Pattern Recognition*, pp. 5107–5116, 2015.
- Minghao Yin, Zhuliang Yao, Yue Cao, Xiu Li, Zheng Zhang, Stephen Lin, and Han Hu. Disentangled non-local neural networks. In Andrea Vedaldi, Horst Bischof, Thomas Brox, and Jan-Michael Frahm (eds.), *Computer Vision – ECCV 2020*, pp. 191–207, Cham, 2020. Springer International Publishing. ISBN 978-3-030-58555-6.
- Changqian Yu, Jingbo Wang, Changxin Gao, Gang Yu, Chunhua Shen, and Nong Sang. Context prior for scene segmentation. In *Proceedings of the IEEE/CVF Conference on Computer Vision and Pattern Recognition*, pp. 12416–12425, 2020a.
- Tianhe Yu, Saurabh Kumar, Abhishek Gupta, Sergey Levine, Karol Hausman, and Chelsea Finn. Gradient surgery for multi-task learning. *Advances in Neural Information Processing Systems*, 33: 5824–5836, 2020b.

- Yuhui Yuan and Jingdong Wang. Ocnet: Object context network for scene parsing. *arXiv preprint arXiv:1809.00916*, 2018.
- Yuhui Yuan, Xilin Chen, and Jingdong Wang. Object-contextual representations for semantic segmentation. In *Computer Vision–ECCV 2020: 16th European Conference, Glasgow, UK, August 23–28, 2020, Proceedings, Part VI 16*, pp. 173–190. Springer, 2020a.
- Yuhui Yuan, Jingyi Xie, Xilin Chen, and Jingdong Wang. Segfix: Model-agnostic boundary refinement for segmentation. In *European Conference on Computer Vision*, pp. 489–506. Springer, 2020b.
- Mingmin Zhen, Shiwei Li, Lei Zhou, Jiaxiang Shang, Haoan Feng, Tian Fang, and Long Quan. Learning discriminative feature with crf for unsupervised video object segmentation. In *European Conference on Computer Vision*, pp. 445–462. Springer, 2020a.
- Mingmin Zhen, Jinglu Wang, Lei Zhou, Shiwei Li, Tianwei Shen, Jiaxiang Shang, Tian Fang, and Long Quan. Joint semantic segmentation and boundary detection using iterative pyramid contexts. In *Proceedings of the IEEE/CVF Conference on Computer Vision and Pattern Recognition*, pp. 13666–13675, 2020b.
- Shuai Zheng, Sadeep Jayasumana, Bernardino Romera-Paredes, Vibhav Vineet, Zhizhong Su, Dalong Du, Chang Huang, and Philip HS Torr. Conditional random fields as recurrent neural networks. In *Proceedings of the IEEE international conference on computer vision*, pp. 1529–1537, 2015.
- Sixiao Zheng, Jiachen Lu, Hengshuang Zhao, Xiatian Zhu, Zekun Luo, Yabiao Wang, Yanwei Fu, Jianfeng Feng, Tao Xiang, Philip HS Torr, et al. Rethinking semantic segmentation from a sequence-to-sequence perspective with transformers. In *Proceedings of the IEEE/CVF conference on computer vision and pattern recognition*, pp. 6881–6890, 2021.
- Bolei Zhou, Hang Zhao, Xavier Puig, Sanja Fidler, Adela Barriuso, and Antonio Torralba. Scene parsing through ade20k dataset. In *Proceedings of the IEEE conference on computer vision and pattern recognition*, pp. 633–641, 2017.
- Lanyun Zhu, Deyi Ji, Shiping Zhu, Weihao Gan, Wei Wu, and Junjie Yan. Learning statistical texture for semantic segmentation. In *Proceedings of the IEEE/CVF Conference on Computer Vision and Pattern Recognition*, pp. 12537–12546, 2021.
- Zhen Zhu, Mengde Xu, Song Bai, Tengpeng Huang, and Xiang Bai. Asymmetric non-local neural networks for semantic segmentation. In *Proceedings of the IEEE/CVF International Conference on Computer Vision*, pp. 593–602, 2019.

A APPENDIX

A.1 FORMULA DERIVATION

Firstly, we give the gradient equation of ∇W_c mentioned in this paper:

$$\nabla W_c = \frac{\partial L_k}{\partial W_c} = \frac{\partial L_k}{\partial P_k^c} \cdot \frac{\partial P_k^c}{\partial Y_k^c} \cdot \frac{\partial Y_k^c}{\partial W_c}. \quad (16)$$

According to it, we present the derivative of each term respectively:

$$\frac{\partial L_k}{\partial P_k^c} = -\frac{1}{P_k^c}, \quad (17)$$

$$\frac{\partial P_k^c}{\partial Y_k^c} = \frac{((\sum_{m \neq c} e^{Y_k^m}) + e^{Y_k^c}) \cdot e^{Y_k^c} - (e^{Y_k^c})^2}{((\sum_{m \neq c} e^{Y_k^m}) + e^{Y_k^c})^2} = \frac{e^{Y_k^c}}{(\sum_{m \neq c} e^{Y_k^m}) + e^{Y_k^c}} - \left(\frac{e^{Y_k^c}}{(\sum_{m \neq c} e^{Y_k^m}) + e^{Y_k^c}}\right)^2, \quad (18)$$

and

$$\frac{\partial Y_k^c}{\partial W_c} = F_k. \quad (19)$$

Further, it is worth noting that P_k^c is given by:

$$P_k^c = \frac{e^{Y_k^c}}{(\sum_{m \neq c} e^{Y_k^m}) + e^{Y_k^c}}. \quad (20)$$

To simplify Eq (18), we take Eq (20) into account. Thus, Eq (18) is formulated as:

$$\frac{\partial P_k^c}{\partial Y_k^c} = P_k^c - P_k^c \cdot P_k^c = P_k^c \cdot (1 - P_k^c). \quad (21)$$

So after integrating Eq (17), Eq (21), and Eq (19), Eq (16) can be formulated as:

$$\nabla W_c = \frac{\partial L_k}{\partial W_c} = -\frac{1}{P_k^c} \cdot P_k^c \cdot (1 - P_k^c) \cdot F_k = -(1 - P_k^c) \cdot F_k. \quad (22)$$

Finally, the class weights W_c^* in the next iteration will be updated:

$$W_c^* = W_c - \nabla W_c = W_c + (1 - P_k^c) \cdot F_k. \quad (23)$$

A.2 EXPERIMENT SETUP

ADE20K ADE20K (Zhou et al., 2017) is one of the most challenging benchmarks, containing 150 fine-grained semantic concepts and a variety of scenes with 1,038 image-level labels. There are 20210 images in training set and 2000 images in validation set.

Cityscapes Cityscapes (Cordts et al., 2016) has 5,000 images captured from 50 different cities. Each image has 2048×1024 pixels, which have high quality pixel-level labels of 19 semantic classes. There are 2,975 images in training set, 500 images in validation set and 1,525 images in test set. We do not use coarse data in our experiments.

Pascal Context PASCAL Context (Mottaghi et al., 2014) is a challenging scene understanding dataset, which provides the semantic labels for the images. There are 4,998 images for training and 5,105 images for validation on PASCAL Context dataset. In our experiment, the 59 most frequent categories are used for training.

Implementation Details. The initial learning rate is set as 0.01 for both datasets. We employ a poly learning rate strategy where the initial learning rate is multiplied by $(1 - iter/totaliter)^{0.9}$ after each iteration. We set training time to 80000 iterations for ADE20K and Pascal Context, and 180 epochs for Cityscapes. Momentum and weight decay coefficients are set as 0.9 and 0.0005, respectively. For data augmentation, we apply the common scale (0.5 to 2.0), cropping and flipping of the image to augment the training data. Input size for ADE20K dataset is set to 512×512 , and 480×480 is for Pascal Context while input size for Cityscapes dataset is set to 832×832 . The syncBN (Peng et al., 2018) is adopted in all experiments, and batch size on ADE20K and Pascal Context is set to 16 and it is set to 8 for Cityscapes.

A.3 COMPARISONS WITH RELATED METHODS ON CITYSCAPES

To further evaluate our proposed method, we thoroughly compare our approach with baseline and other traditional CRF-based methods, *i.e.*, Vanilla-CRF and Joint-CRF on Cityscapes dataset. As shown in Table 5, E-CRF achieves the best result among all those methods, which outperforms the baseline model by **0.92%** in mIoU and **3.81%** in F-score respectively. Obviously, our method is more effective than both Vanilla-CRF and Joint-CRF.

Method	ResNet-50		ResNet-101	
	F-score (%)	mIoU (%)	F-score (%)	mIoU (%)
DeeplabV3+	60.48	79.54	61.94	80.85
Vanilla-CRF	62.38	79.65 (+0.11)	63.46	80.92 (+0.07)
Joint-CRF	63.44	79.78 (+0.24)	64.43	81.05 (+0.20)
E-CRF (Ours)	64.29	80.35 (+0.81)	65.57	81.77 (+0.92)

Table 5: Comparisons with baseline, Valina-CRF and Joint-CRF on Cityscapes *val* dataset.

A.4 MORE ABLATION STUDIES

A.4.1 DIFFERENT BOUNDARY REFINEMENT

We consider three typical methods including Segfix Yuan et al. (2020b), DecoupleSegNet Li et al. (2020b), and ABL⁶ (Wang et al., 2022). They refine boundary segmentation via post-processing, improving boundary representation, and adding boundary alignment loss respectively. But all of them ignore the existence of BCWC issue, which may restrict their capability. In Table 4, we use DeeplabV3+ with ResNet101 as our baseline method. For Segfix, we use the official code (It uses HRNet as backbone) to boost the performance of DeeplabV3+. For DecoupleSegNet which is constructed based on DeeplabV3+, we also use the official code (It uses ResNet101 as backbone). All the models are trained on ADE20K for 80K iterations with batch size set to 16. When testing, we adopt the single-scale testing strategy (*i.e.*, raw image) because using a single scale (*i.e.*, raw images) when comparing with baselines or performing ablation studies is a traditional default setting in the semantic segmentation field. The goal is to eliminate the effect of other elements (*e.g.*, image augmentation).

It is observed that all the methods enhance the performance and E-CRF achieves the highest mIoU and F-score. We speculate that this is because E-CRF has explicitly considered the BCWC problem and optimizes the class weights from both scale and direction aspects while refining boundary representation. It also indicates the importance of obtaining distinguishable class weights in semantic segmentation.

Table 6: Comparisons with other boundary refining methods on ADE20K *val* dataset.

Method	mIoU (%)	F-score (%)
DeeplabV3+ (Chen et al., 2018a)	44.60	16.15
SegFix (Yuan et al., 2020b)	45.62	18.14
DecoupleSegNet (Li et al., 2020b)	45.73	18.02
ABL (Wang et al., 2022)	45.38	-
E-CRF	46.02	18.32

A.4.2 COMPARISONS ON COMPUTATIONAL COSTS

We take DeeplabV3+ based on ResNet101 as the baseline model to perform the training time comparisons. Image size is set to 512×512 and all the experiments are conducted on 8 GeForce RTX 2080Ti GPU's with two images per GPU. The FLOPs, parameter size, and inference FPS are also reported in Table 7. We can find that our proposed E-CRF brings negligible extra costs over the baseline model. The cost difference between E-CRF and Joint-CRF is marginal. We also measure the time consuming of superpixel method (**5ms**), which is much smaller than that of inference (**55ms**).

⁶The authors do not provide the code in their paper. Hence, we just report the result based on OCRNet (Yuan et al., 2020a) in their paper.

Table 7: Comparisons on Computational costs on ADE20K dataset.

Method	Backbone	Training Time(s)	FLOPs(G)	Parameters(M)	FPS
DeeplabV3+	ResNet101	0.71	254.8	60.1	19.75
Vanilla-CRF	ResNet101	0.71	254.8	60.1	1.86
Joint-CRF	ResNet101	0.73	254.9	60.2	19.04
E-CRF	ResNet101	0.74	255.0	60.2	18.32

A.5 DISCUSSION

In this section, we discuss the difference between E-CRF and three related works including PCGrad (Yu et al., 2020b), OCNet (Yuan & Wang, 2018), and SegFix (Yuan et al., 2020b).

Difference between Projecting Conflicting Gradients (PCGrad) and E-CRF: PCGrad and E-CRF are both gradient-based methods that focus on adjusting the gradient properly to optimize the learning process more effectively and efficiently. PCGrad is designed to mitigate a key optimization issue in multi-task learning caused by conflicting gradients, where gradients for different tasks point away from one another as measured by a negative inner product. If two gradients are conflicting, PCGrad alters the gradients by projecting each onto the normal plane of the other, preventing the interfering components of the gradient from being applied to the network. The idea behind PCGrad is simple and the method is effective. PCGrad is a task-level gradient optimization method, mainly focusing on conflicting gradients caused by multiple tasks during training (*e.g.*, in semantic segmentation and depth estimation). E-CRF is a finer-grained pixel-level gradient optimization method. E-CRF mainly aims at mitigating the boundary-caused class weights confusion in semantic segmentation via adjusting class weights from both scale and direction.

Difference between OCNet and E-CRF: OCNet uses self-attention to implement the object context pooling module. The object context pooling estimates the context representation of each pixel by aggregating the representations of the selected subset of pixels based on the estimated dense relation matrix. Further, OCNet combines context pooling module with the conventional multi-scale context schemes including PPM and ASPP. In E-CRF, we follow the idea behind Conditional Random Field and embed it from logit space to deep-feature space. We instance the unary function and reformulate the pairwise function with a convolutional-based kernel. The kernel takes raw image RGB value and relative position embeddings as inputs (See Eq (6)), which is different from self-attention that takes extracted deep features as inputs. We also maintain one special term in CRF called label compatibility and transfer it to feature compatibility (See Eq (7)). Such is missing in self-attention. Besides, we do not measure the similarity between superpixel center and boundary pixels. We simply leverage the local prior in superpixel and use it to guide deep feature averaging. The motivation is to suppress noise information. Finally, the motivation between OCNet and E-CRF is different. OCNet mainly focuses on integrating as much object context as possible while E-CRF explicitly targets on the BCWC problem and optimizes class weights from both scale and direction.

Difference between SegFix and E-CRF: SegFix first encodes input image and predicts a boundary map and a direction map. Then SegFix uses the predicted boundary map and offset map derived from the direction map to correct the wrongly classified boundary pixels via internal points with high confidence. SegFix is beneficial for refining boundary segmentation and is served as a post-processing method, thus lacking the capability to alleviate BCWC problem. Our method is derived from traditional CRF (a post-processing method) and can be regarded as a plug-and-play module. It can be easily integrated with other methods. Besides, our method extends the optimization flexibility for BCWC problem. Empirically, we have compared Segfix and E-CRF based on DeeplabV3+ in Table 6 (Please see A.4.1). E-CRF produces 46.02% for mIoU on ADE20K, outperforming SegFix (45.62%) by 0.4%. This indicates the importance of alleviating BCWC problem.

A.6 PAIRWISE MESSAGE PASSING VISUALIZATION

E-CRF takes an equivalent transformation to replace hand-designed Gaussian kernels in Vanilla-CRF with simple convolution operators for more flexible end-to-end optimization. The convolution operation involves two aspects. One is the appearance similarity and the other one is the relative position between pixels. As depicted in Fig 4(a), we take a pixel k in the stool for an example and

show its relationship with other pixels in the image. Fig 4(b) and Fig 4(c) show its appearance similarity and *cosine* position embedding with other pixels respectively. It is clear that pixels share similar colors or close to the target pixel k tend to be highlighted. Subsequently, in Fig 4(d), we directly visualize the results of our pairwise message passing module ψ_p^f defined in Eq.(5). We can find that ψ_p^f becomes concentrated on the most relevant pixels compared with the pixel k , which verifies the reliability of our pairwise message passing design.

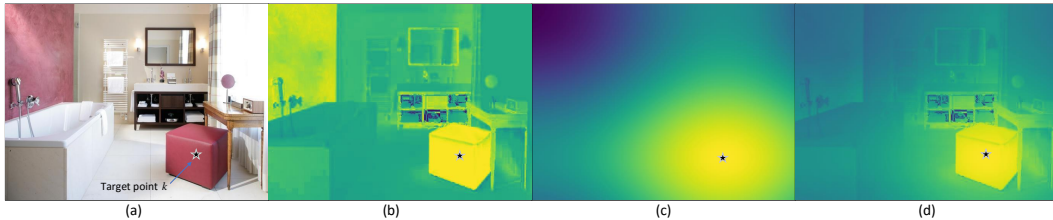


Figure 4: Visualization of pairwise message passing module ψ_p^f in E-CRF. **(a)** A target pixel k of the stool in the image. **(b)** The appearance similarity between other pixels and k . Pixels share the similar colors with k tend to be highlighted. **(c)** The visualization of the relative position between k and other pixels. Pixels close to k achieve higher values. **(d)** The visualization of ψ_p^f in E-CRF. ψ_p^f focuses more on most relevant pixels compared to k .

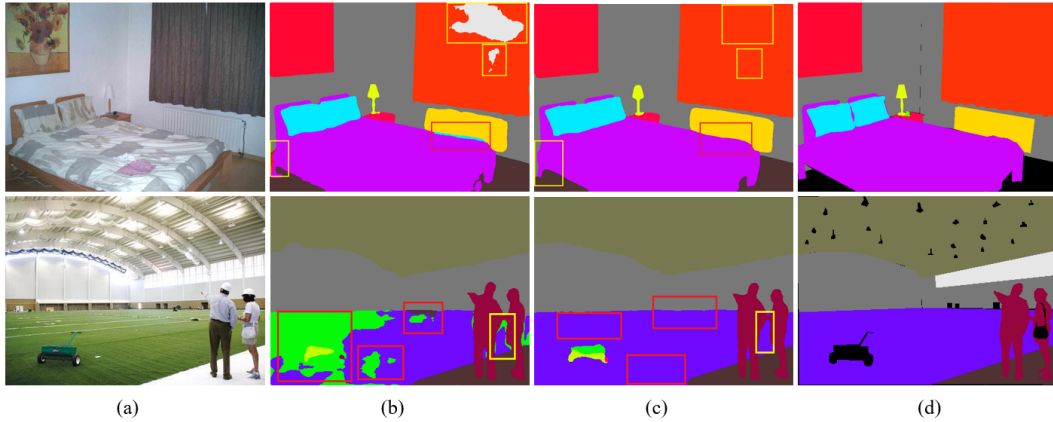


Figure 5: Visualization comparisons between our method and baseline on ADE20K validation set. **(a)** Images from ADE20K dataset. **(b)** Segmentation output from DeeplabV3+. **(c)** Segmentation output from our method. Obviously, compared with baseline, the results are segmented well by E-CRF. **(d)** Image labels.

B BCWC IN TRANSFORMER

Are transformer-based models also suffering from Boundary-caused Class Weight Confusion? Is our method effective to transformer-based models? To answer these questions, we make a preliminary exploration in this section.

B.1 OBSERVATIONS ON ADE20K

Following the same idea in Fig.1(a) of this paper, we take Segformer (Xie et al., 2021) (a transformer-based segmentation model) as an example to train on ADE20K (Zhou et al., 2017) dataset. We count the number of adjacent pixels for each class pair and find a corresponding category that has the most adjacent pixels for each class. Then, we calculate the similarity of their class weights and depict it in Fig 6. X-axis stands for the number of adjacent pixels for each class pair in descending order, and Y-axis represents the similarity of their class weights. Blue line denotes Segformer while orange line denotes E-CRF based on Segformer. As shown

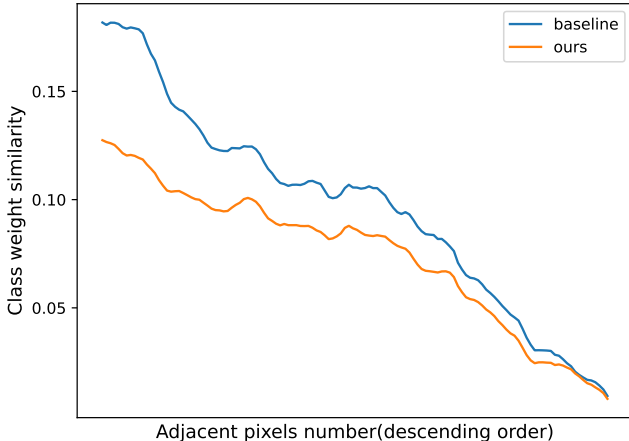


Figure 6: Class weight similarity on transformer-based model

in Fig 6, two categories that share more adjacent pixels are inclined to have more similar class weights, while E-CRF effectively decreases the similarity between adjacent categories and makes their class weights more discriminative. These observations on transformer-based model are quite similar to previous results in CNN-based models. Apparently, transformer-based models are also suffering from Boundary-caused Class Weight Confusion.

B.2 EFFECTIVENESS ON TRANSFORMER

To evaluate the effectiveness of our method, we take Segformer (Xie et al., 2021) (based on MiT-B5) as our transformer baseline and incorporate E-CRF into it. Experiments are conducted on ADE20K and Cityscapes datasets. Similarly, we also compare our method with other traditional CRF-based methods, *i.e.*, Vanilla-CRF and Joint-CRF⁷. As shown in Table 8, E-CRF achieves the best result among all those methods, which surpasses the baseline model with up to **1.01%** mIoU and **3.81%** F-score improvements. By E-CRF relieves the disturbing gradients caused by the BCWC problem boost the overall segmentation performance and the boundary segmentation. Fig 6 also proves that E-CRF can decrease the inter-class similarity consistently which results in more discriminative feature representations.

Method	ADE20K		Cityscapes	
	F-score (%)	mIoU (%)	F-score (%)	mIoU (%)
Segformer	18.53	49.13	62.42	82.25
Vanilla-CRF	21.72	49.36 (+0.23)	64.06	82.31 (+0.06)
Joint-CRF	21.91	49.55 (+0.42)	64.93	82.41 (+0.16)
E-CRF (Ours)	22.34	50.14 (+1.01)	66.05	83.07 (+0.82)

Table 8: Comparisons with baseline, Valina-CRF, and Joint-CRF on ADE20K and Cityscapes *val* datasets.

⁷Note that they are also based on Segformer

B.3 COMPARISONS WITH SOTA METHODS

To further verify the effectiveness, we compare our methods with other transformer-based SOTA methods with similar number of parameters (except SETR) for fair comparisons in both ADE20K and Cityscapes datasets. Multi-scale testing and left-right flipping strategies are adopted. As shown in Table 9, our method achieves the best results among all the SOTA methods in both ADE20K and Cityscapes datasets. Besides, our method also has the smallest number of parameters.

Table 9: Comparisons with other transformer-based SOTA methods on ADE20K *val* dataset and Cityscapes *val* and *test* dataset.

Method	Backbone	mIoU(%)			Params (M)
		ADE- <i>val</i>	City- <i>val</i>	City- <i>test</i>	
SETR (Zheng et al., 2021)	ViT-L (307M)	50.20	82.15	82.2	310M
UperNet	Swin-B (Liu et al., 2021) (88M)	49.65	-	-	121M
UperNet	Twins-L (Chu et al., 2021) (99M)	50.20	-	-	133M
SegFormer (Xie et al., 2021)	MiT-B5 (81M)	50.22	83.48	82.2	85M
UperNet	XCiT-M24 (Chu et al., 2021) (84M)	48.40	-	-	109M
DPT (Ranftl et al., 2021)	ViT-B (86M)	48.34	-	-	112M
Segmentor (Strudel et al., 2021)	DeiT-B (86M)	50.08	80.60	-	86M
E-CRF (Ours)	MiT-B5 (81M)	51.28	83.7	82.5	85M